Adaptive Active Fault-Tolerant MPPT Control of Variable-Speed Wind Turbine Considering Generator Actuator Failure

Jian Chen[a], Wei Yao[b,*], Qun Lu[a], Yaxing Ren[c], Wenyong Duan[a], Jiarong Kan[a], Lin Jiang[c]

[a]*School of Electrical Engineering, Yancheng Institute of Technology, Yancheng, 224051, China*
[b]*State Key Laboratory of Advanced Electromagnetic Engineering and Technology, School of Electrical and Electronics Engineering, Huazhong University of Science and Technology, Wuhan, 430074, China*
[c]*Department of Electrical Engineering and Electronics, University of Liverpool, Liverpool, L69 3GJ, United Kingdom.*

Abstract

In order to ensure that the wind power system (WPS) can realize maximum power point tracking (MPPT) under generator side fault, an MPPT control system with adaptive active fault tolerance capability is proposed in this paper. The basic idea of the proposed control strategy is that a perturbation term containing model uncertainties, system nonlinearities and unknown disturbances (generator actuator failure and disturbance torque) is estimated in real-time by a designed observer. The estimated perturbation is used for the compensation of actual perturbation. Then, an adaptive feedback linearizing control of variable-speed wind turbine (VSWT) system can be realized. Therefore, the control strategy neither requires detailed system model and full state measurements, nor relies on fault detection, diagnosis and isolation techniques when the generator actuator fails. Simulation results show that the proposed control scheme has smaller tracking error and better dynamic performance than the traditional PI control and MPPT control, and higher robustness against system parameter uncertainties, disturbance torque and generator actuator failure than the nonlinear static state feedback based MPPT (NSSF-MPPT) control, traditional PI control and MPPT control.

Keywords: Wind power system, adaptive active fault-tolerant MPPT control, nonlinear adaptive control, generator actuator failure, maximum power point tracking

Nomenclature

AAFT-MPPTC	adaptive active fault-tolerant MPPT control	HGO	high-gain observer
ADRC-MPPT	active disturbance rejection control based MPPT	ITAE	integral of the time multiplied by the absolute error
AFTC	active fault-tolerant control	MPPT	maximum power point tracking
FDI	fault diagnosis and isolation	MPPT-OTSR	MPPT control based on OTSR
HCS	hill climb searching	MRE	maximum regulation error

*Corresponding Author: W. Yao, Tel.: +86 13657247542, Email: w.yao@hust.edu.cn

July 6, 2022

NSSF-MPPT	nonlinear static state feedback based MPPT	SMPO-NAC	NAC based on sliding-mode perturbation observer
ORS	optimal rotation speed	VSWT	variable-speed wind turbine
ORSE	ORS estimation	WPS	wind power system
OTSR	optimal tip speed ratio	WPSs	wind power systems
PSF	power signal feedback	WT	wind turbine

1. Introduction

Efficient and stable operation is important for reducing wind farm operation and maintenance costs and successful deployment of wind power systems (WPSs) [1, 2]. The costs can be effectively reduced by improving the efficiency of WPSs [3, 4]. More than 50% of the energy for a variable-speed wind turbine (VSWT) is captured in the operation area below the rated wind speed. Therefore, it is particularly important to improve the efficiency of a VSWT by maximum power point tracking (MPPT) control [5, 6]. At the same time, a wind turbine (WT) will inevitably encounter some faults after operating a long period in the severe environment. As the actuator of the speed control, the generator of a WPS is one of the components most prone to failure. In the operation period of WPSs, the execution efficiency may be decreased under generator actuator failure. If the WPS is controlled in accordance with the original MPPT control strategy, it is bound to affect the performance of the WPS and even lead to system instability and serious accidents [7, 8]. Therefore, considering the failure of generator actuator in the MPPT control strategy is crucial to ensure safety performance and reduce costs [2, 8].

In the WPS, the MPPT control strategy makes the VSWT always operate on the optimal tip speed ratio (OTSR) through the adjustment of VSWT speed, so as to realize the capture of maximum wind energy [9]. In the traditional MPPT control strategies, it can be mainly divided into the following three kinds: hill climb searching (HCS) method [10, 11, 12], power signal feedback (PSF) method [13, 14] and OTSR method [15, 16, 17, 18, 19]. To overcome the problems of step size selection, speed oscillation and search direction misjudgment existing in the conventional HCS algorithm, a new peak detection method has been designed to keep up with the rapidly varying wind speed by changing the step size and overcome the drawback of speed oscillation at the maximum power point [10]. The optimized HCS method has solved the problem of searching direction [11]. Generally, compared with large inertia VSWTs with slow response, the HCS is more suitable for small and medium-sized VSWTs [12, 20]. Due to the high turbulence intensity of wind speed and slow response of large inertia VSWT, the traditional PSF control strategy needs a certain time to achieve the optimal speed, which reduces the efficiency of the VSWT [20]. To increase the efficiency of the conventional PSF control strategy, the researchers have proposed the MPPT control strategies based on the tracking range reduction [13] and adaptive torque control method [14]. However, these methods are inseparable from offline training, and need to obtain the optimal starting speed according to the recorded wind speed data. Because the

rotation speed is adjusted directly according to the feedback of speed error, the MPPT control based on OTSR (MPPT-OTSR) has faster response speed than the MPPT control based on PSF and HCS [20]. The MPPT-OTSR can quickly track the optimal rotation speed (ORS) under high turbulence wind speed, so as to capture wind energy efficiently [15, 16]. Conventional OTSR requires real-time observation of wind speed to achieve the ORS. In the wind farm, the wind speed is often measured by the anemometer at a certain point. However, considering the huge sweeping area of the large inertia VSWT, the equivalent wind speed acting on the VSWT cannot be simply replaced by the measured wind speed [21]. Hence, accurate estimation of the equivalent wind speed for obtaining the ORS estimation (ORSE) plays an important role in effective wind energy capture [22]. In this paper, the ORSE is obtained according to the estimated wind speed, which has been designed in author's previous research work [23]. Although literatures [17, 18, 19] realized MPPT based on estimated wind speed or ORSE, they focus on high efficiency without considering the influence of generator actuator failure, parameter uncertainties and unknown disturbances on the control system. The design of MPPT control strategy considering the impact of generator actuator failure is critical to ensure system safety and reduce maintenance cost, but there is a lack of research in this aspect [7, 8].

Fault-tolerant capability is important for the decrement of the WT downtime and fault detection. The active fault-tolerant control (AFTC) approach is based on the controller with capability of resetting parameters or even modifying the structure, and realizes a fast dynamic compensation of control outputs after failures, so as to keep the system stable. Therefore, in case of failure, the AFTC must actively provide corresponding failure or state information. In the design of AFTC, fault diagnosis and isolation (FDI) technology is an important method. The FDI methods have been widely used in WPSs, including fuzzy modeling method [2, 24], varying parameter method [25], Kalman filtering method [26], robust fuzzy method [27], observation method [28, 29, 30], data-driven method [31], deep learning [32] and so on. Refs. [25, 30, 31, 32] mainly pay attention to the detection, diagnosis, isolation and estimation of the VSWT failures, rather than the fault-tolerant control (FTC) system of the VSWTs after failures.

To ensure the efficient realization of AFTC through FDI technology after VSWT failures, a new method using fuzzy modeling, identification and fault diagnosis has been proposed in [24], which ensures the normal operation of VSWTs in the case of the failures of generator speed and pitch angle sensors. When the stator current sensor of the doubly-fed WT fails, the closed-loop control system is reconstructed by FDI technology to ensure the efficient operation of the VSWT at time-varying wind speed [26]. Ref. [27] has successfully realized the speed tracking control under the failure of speed sensor by comparing the differences between measurements and estimations of state variables. In the case of sensor and generator actuator failures, a fault estimation method is used to keep the controller in a satisfactory working state [28]. For the converter failure, Ref. [29] ensures the safe operation of WPS through fault detection and reconstruction of control system. Based on the construction principle of control system, the FDI technology is used to process failure information accurately, which makes the AFTC have strong robustness and adaptability. However, when the AFTC relies heavily on the performance of FDI, the fault-tolerant ability of AFTC may even be lower than that of passive FTC because of failure detection omission, large diagnostic error or long time delay caused by fault diagnosis mechanism [2].

To avoid relying on the performance of FDI, adaptive control output compensation technology is applied to AFTC strategy, which has attracted more and more attention. The control strategy only uses the variations of system state variables caused by failures to provide the required failure information for the controller. This method has been applied in the FTC of WPSs due to its obvious advantage of fast fault compensation [7, 8, 33, 34]. In [33], an adaptive output feedback sliding-mode controller for pitch control has been proposed to enhance the fault-tolerant capability of the control system against the generator actuator failure without knowing failure information. However, its research object is the pitch control system. In [7, 8], the adaptive AFTC strategies based on MPPT have been adopted to deal with generator actuator failure, modeling error and external disturbances, without requiring failure information detection. However, the differential of rotor speed is required to be known in [7], and the online estimation of some control system parameters is needed in [8]. In [34], it has proposed a robust AFTC method based on power tracking control and distributed control scheme, which ensures the transient performance of each VSWT in the wind farm and robustness against generator actuator failure. However, the relevant parameters need to be estimated online. At present, there are few literatures on the application of adaptive AFTC in MPPT control strategy for VSWT to solve generator actuator failure. Therefore, an adaptive active fault-tolerant MPPT control (AAFT-MPPTC) strategy has been developed to deal with the uncertainties that may occur in VSWTs, including potential generator actuator failure, system model uncertainties and external disturbance.

An MPPT control strategy designed based on OTSR of the VSWT with adaptive active fault-tolerant capability is proposed in this paper. The factors such as system nonlinearities, model uncertainties, external disturbance and generator actuator failure are considered in the proposed control strategy. In this control strategy, the Newton-Rafson iterative method is used to obtain the estimation of wind speed, which avoids the use of wind speed measurement device. In the control system design, by defining a perturbation of VSWT system to represent the nonlinearities, uncertainties of the model and unknown disturbances (including disturbances caused by generator actuator failure and disturbance torque), a designed observer is employed for real-time observation of perturbation to compensate actual perturbation. The adaptive linearization of the original VSWT system is realized, and only few system state variables need to be known. In the case of generator actuator failure, the design of control strategy avoids the reset of controller parameters and structure change, as well as the use of relevant fault detection and diagnosis technologies. The simulation test scenarios include time-varying wind speed, parameter uncertainty, disturbance torque and generator actuator failure. The proposed control strategy is compared with the nonlinear static state feedback based MPPT (NSSF-MPPT) control, traditional PI control and MPPT control methods. The simulation results show that the AAFT-MPPTC not only ensures high dynamic performance and efficiency, but also provides strong robustness against parameter uncertainty and disturbance torque, and satisfactory fault tolerance for generator actuator failure.

The main relation and difference of this work with previously published works [16], [41], [42] are summarized as follows:

- In [16], [41] and [42], the research objects are the permanent magnet synchronous generator, grid-side inverter,

and permanent magnet synchronous motor, respectively. The research object of this paper is the WT.

- In [16], it pays more attention to MPPT, and pursues the fast tracking of the optimal speed and ignores the slow response of large inertia WT. In [41], the main objective is designing a controller for the grid-side inverter to improve the low-voltage ride-through capability (LVRTC) of the WPS. In [42], the main objectives are tracking mechanical rotation speed and providing high robustness against system parameter uncertainties and unknown fast varying load torque disturbance. The main objective of this paper not only pursues high efficiency, but also considers the slow response characteristics of WT and generator actuator failure.

- In [16], the MPPT is achieved by controlling rotor speed and current via the generator-side converter. The optimal rotor speed is obtained based on wind speed measured by anemometer. In [41], the LVRTC is improved by regulating the DC-link voltage and current. The detailed model of the generator-side inverter, generator and WT has not presented in this research work. In [42], the mechanical rotation speed and current are regulated to provide high robustness against uncertainties and disturbances. This paper is based on Newton-Raphson iterative method to obtain real-time wind speed without using anemometer. This paper not only pursues high efficiency, but also considers the slow response characteristics of WT, influence of generator actuator failure and disturbance torque in the design of MPPT controller.

The main contributions of this paper can be listed as follows,

- To maximize the wind energy capture of VSWT under time-varying wind speed, the perturbation estimation techniques are used for AAFT-MPPTC to track the optimal rotor speed, whose effectiveness has been verified by simulation tests. Meanwhile, the ORSE is obtained by the estimated wind speed, so the anemometer is omitted.

- The designed observer can fully consider all VSWT nonlinearities, uncertainties and unknown disturbances without requiring detailed system model. Thus, the proposed AAFT-MPPTC strategy can robust against uncertainties and unknown disturbance (disturbance torque and generator actuator failure).

- The proposed AAFT-MPPTC approach is an output feedback controller, which does not require full state measurements, so it is easy to be implemented in practical systems.

The remaining of this paper is organized as follows: Section 2 briefly recalls the VSWT model. In Section 3, the proposed AAFT-MPPTC of the VSWT is designed. Simulation case studies are undertaken to verify the proposed controller performance in Section4, and compare it with the NSSF-MPPT, MPPT, traditional PI and other observer based controllers. Finally, Section 5 gives the conclusions of this paper.

2. Model of the VSWT and Problem Formulation

2.1. Model of the VSWT

The aerodynamic power captured by the VSWT is as follows

$$P_{\mathrm{a}} = \frac{1}{2}\rho\pi R^2 V^3 C_{\mathrm{p}}(\beta, \lambda) \tag{1}$$

where, V is the wind speed, R is the blade radius, ρ is the air density, β is the pitch angle, $C_{\mathrm{p}}(\beta, \lambda)$ is the power coefficient, and the tip speed ratio (TSR) λ is defined as follows

$$\lambda = \frac{\omega_{\mathrm{r}} R}{V} \tag{2}$$

where, the rotor speed is ω_{r}.

The power coefficient C_{p} of the VSWT is a function of pitch angle β and TSR λ. In this paper, the C_{p} recalled from [35, 36] is expressed as follows

$$C_{\mathrm{p}}(\beta, \lambda) = 0.22\left(\frac{116}{\lambda_t} - 0.4\beta - 5\right)e^{\frac{-12.5}{\lambda_t}} \tag{3}$$

where

$$\lambda_t = \frac{1}{\lambda + 0.08\beta} - \frac{0.035}{\beta^3 + 1} \tag{4}$$

Fig. 1 shows the configuration of a simplified model for VSWT. The state-space model of the VSWT [7, 8, 35] is expressed as

$$\dot{x} = f(x) + g(x)u = \begin{bmatrix} f_1(x) \\ f_2(x) \\ f_3(x) \end{bmatrix} + \begin{bmatrix} g_{11} \\ g_{21} \\ g_{31} \end{bmatrix} u \tag{5}$$

where

$$f(x) = \begin{bmatrix} f_1(x) \\ f_2(x) \\ f_3(x) \end{bmatrix} = \begin{bmatrix} l_{11} & l_{12} & l_{13} & l_{14} \\ l_{21} & l_{22} & l_{23} & l_{24} \\ l_{31} & l_{32} & l_{33} & l_{34} \end{bmatrix},$$

$$\begin{aligned}
&g_{11} = 0, && g_{21} = -\tfrac{1}{J_{\mathrm{g}}}, && g_{31} = \tfrac{D_{\mathrm{s}}}{N_{\mathrm{g}} J_{\mathrm{g}}}, \\
&l_{11} = -\tfrac{K_{\mathrm{r}}}{J_{\mathrm{r}}}, && l_{21} = 0, && l_{31} = K_{\mathrm{s}} - \tfrac{D_{\mathrm{s}} K_{\mathrm{r}}}{J_{\mathrm{r}}}, \\
&l_{12} = 0, && l_{22} = -\tfrac{K_{\mathrm{g}}}{J_{\mathrm{g}}}, && l_{32} = -\tfrac{1}{N_{\mathrm{g}}}(K_{\mathrm{s}} - \tfrac{D_{\mathrm{s}} K_{\mathrm{g}}}{J_{\mathrm{g}}}), \\
&l_{13} = -\tfrac{1}{J_{\mathrm{r}}}, && l_{23} = \tfrac{1}{N_{\mathrm{g}} J_{\mathrm{g}}}, && l_{33} = -D_{\mathrm{s}}(\tfrac{J_{\mathrm{r}} + N_{\mathrm{g}}^2 J_{\mathrm{g}}}{N_{\mathrm{g}}^2 J_{\mathrm{g}} J_{\mathrm{r}}}), \\
&l_{14} = \tfrac{1}{J_{\mathrm{r}}}, && l_{24} = 0, && l_{34} = \tfrac{D_{\mathrm{s}}}{J_{\mathrm{r}}}, \\
&x = [\omega_{\mathrm{r}} \quad \omega_{\mathrm{g}} \quad T_{\mathrm{ls}}]^{\mathrm{T}}, && y = \omega_{\mathrm{r}}, && u = T_{\mathrm{em}},
\end{aligned}$$

where, $x \in R^3$, $y \in R^1$ and $u \in R^1$ are state vector, output vector and input vector, respectively; $f(x)$ and $g(x)$ are smooth vector fields. D_{s} is the stiffness of low-speed shaft, K_{r} is the external damping of rotor, K_{g} is the external

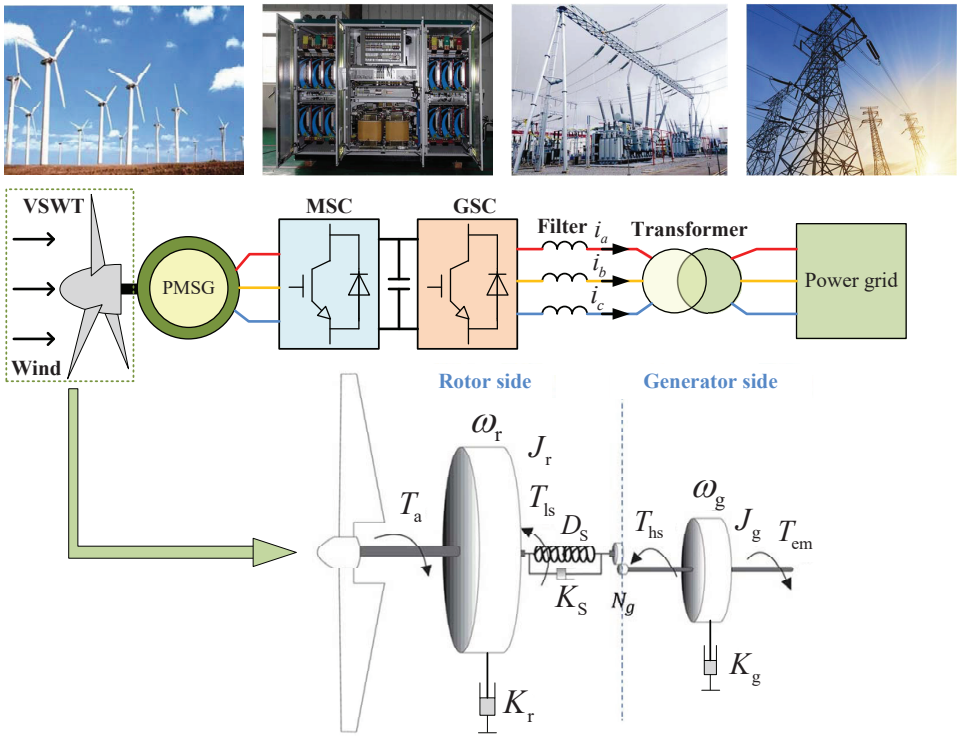

Figure 1: The configuration of a simplified model of VSWT.

damping of generator, J_g is the inertia of generator, K_s is the damping of low-speed shaft, ω_g is the generator speed, J_r is the inertia of rotor, ω_r is the rotor speed, N_g is the gearbox ratio, T_{em} is the generator torque, and T_{ls} is the low-speed shaft torque.

2.2. MPPT Control Strategy Based on OTSR

The objective of the VSWT is maximizing wind power capture when wind speed is between cut-in and rated wind speed, which can be realized by designing an MPPT controller [37]. An MPPT controller adopting OTSR strategy is employed to capture maximum power from time-varying wind. Therefore, it requires that the $C_p(\beta, \lambda)$ should be kept at its maximum value C_{popt} at time-varying wind speed. When the λ reaches its optimal value λ_{opt} at a constant pitch angle β, the maximum value C_{popt} can be achieved. According to (2), when the ORS ω_{ref} is tracked, λ_{opt} can be obtained.

$$\omega_{ref} = \frac{\lambda_{opt} V}{R} \tag{6}$$

It can be seen from Eq. (6) that, when λ_{opt} is constant, wind speed is linear with ω_{ref}. In the wind farm, the wind speed is often measured by the anemometer at a certain point. However, considering the huge sweeping area of the large inertia WT, the equivalent wind speed acting on the WT cannot be simply replaced by the measured wind speed [36]. To obtain the equivalent wind speed, the Newton-Raphson method is employed to estimate wind speed in author's previous research work [23]. For more details, please refer to [23].

2.3. System Model With Generator Actuator Failure

Under normal operation of the VSWT, the maximum wind energy can be extracted by the MPPT controller based on OTSR control strategy. However, some failures are inevitable for WPSs operating in harsh environment, such as converter failure, blade failure, gearbox failure, actuator failure, etc [2, 7, 8]. Among them, wind turbine generator as the speed control actuator is one of the components that is most prone to failure. The failure of the generator actuator leads to the decrement of the efficiency for the generator actuator, and even safety problems[8]. The main reasons of the generator actuator failure are the increment of mechanical friction, looseness of the transmission link, failure of the drive motor, generator phase loss and so on[2, 7, 8]. When the generator actuator failure is considered, the relationship between the designed control input T_{em} and actual control input T_{ga} can be described as follows

$$T_{ga} = \rho(t) T_{em} + \delta_g(t) \tag{7}$$

where $\rho(t)$ is the health indicator, which is a time-varying scalar function with a bounded range $\rho(t)\epsilon(0, 1]$. 0 and 1 respectively indicate that the actuator is completely damaged and without failure [2, 7, 8, 33]. The disturbance torque $\delta_g(t)$ may be caused by friction resistance moment of gear system, generator ripple current, rotor centroid offset and so on, which might be time-varying and immeasurable [7, 8].

3. AAFT-MPPTC Design for the VSWT

3.1. Estimation of Perturbation Considering Generator Actuator Failure

For system (5) without considering generator actuator failure, $T_{\rm em}$ and $\omega_{\rm r}$ are chosen as the input and output, respectively. Define the tracking error $e = \omega_{\rm r} - \omega_{\rm r}^*$, then the second-order derivative of $\ddot{e}$ is obtained as

$$\begin{aligned}\ddot{e} &= \frac{\dot{T}_{\rm r}}{J_{\rm r}} - \frac{(l_{34}J_{\rm r}+K_{\rm r})}{J_{\rm r}^2}T_{\rm r} + \frac{(K_{\rm r}^2 - l_{31}J_{\rm r})}{J_{\rm r}^2}\omega_{\rm r} - \frac{l_{32}}{J_{\rm r}}\omega_{\rm g} \\ &\quad + \frac{(K_{\rm r} - l_{33}J_{\rm r})}{J_{\rm r}^2}T_{\rm ls} + m(x)T_{\rm em} - \ddot{\omega_{\rm r}}^*\end{aligned} \tag{8}$$

where, $m(x) = -\frac{B_{\rm ls}}{N_{\rm g}J_{\rm r}J_{\rm g}} \neq 0$ for all nominal operation points, and $\omega_{\rm r}^* = \omega_{\rm ref}$.

In this paper, the generator actuator failure (7) is considered. Then, the value of $T_{\rm em}$ in (8) should be $T_{\rm ga} = \rho(t)T_{\rm em} + \delta_{\rm g}(t)$. Hence, (8) should be as follows

$$\begin{aligned}\ddot{e} &= \frac{\dot{T}_{\rm r}}{J_{\rm r}} - \frac{(l_{34}J_{\rm r}+K_{\rm r})}{J_{\rm r}^2}T_{\rm r} + \frac{(K_{\rm r}^2 - l_{31}J_{\rm r})}{J_{\rm r}^2}\omega_{\rm r} - \frac{l_{32}}{J_{\rm r}}\omega_{\rm g} \\ &\quad + \frac{(K_{\rm r} - l_{33}J_{\rm r})}{J_{\rm r}^2}T_{\rm ls} + m(x)[\rho(t)T_{\rm em} + \delta_{\rm g}(t)] - \ddot{\omega_{\rm r}}^*\end{aligned} \tag{9}$$

It can also expressed as

$$\begin{aligned}\ddot{e} &= \frac{\dot{T}_{\rm r}}{J_{\rm r}} - \frac{(l_{34}J_{\rm r}+K_{\rm r})}{J_{\rm r}^2}T_{\rm r} + \frac{(K_{\rm r}^2 - l_{31}J_{\rm r})}{J_{\rm r}^2}\omega_{\rm r} - \frac{l_{32}}{J_{\rm r}}\omega_{\rm g} + \frac{(K_{\rm r} - l_{33}J_{\rm r})}{J_{\rm r}^2}T_{\rm ls} \\ &\quad + m(x)[(\rho(t)-1)T_{\rm em} + \delta_{\rm g}(t)] + (m(x)-m_0)T_{\rm em} + m_0T_{\rm em} - \ddot{\omega_{\rm r}}^*\end{aligned} \tag{10}$$

The perturbation term including all system nonlinearities, uncertainties and disturbances (including generator actuator failure and disturbance torque) in (10) is defined as

$$\begin{aligned}\Psi &= \frac{\dot{T}_{\rm r}}{J_{\rm r}} - \frac{(l_{34}J_{\rm r}+K_{\rm r})}{J_{\rm r}^2}T_{\rm r} + \frac{(K_{\rm r}^2 - l_{31}J_{\rm r})}{J_{\rm r}^2}\omega_{\rm r} - \frac{l_{32}}{J_{\rm r}}\omega_{\rm g} + \frac{(K_{\rm r} - l_{33}J_{\rm r})}{J_{\rm r}^2}T_{\rm ls} \\ &\quad + m(x)[(\rho(t)-1)T_{\rm em} + \delta_{\rm g}(t)] + (m(x)-m_0)T_{\rm em}\end{aligned} \tag{11}$$

where, the constant control gain $m_0 = -\frac{B_{\rm ls0}}{N_{\rm g}J_{\rm r0}J_{\rm g0}}$. $B_{\rm ls0}$, $J_{\rm r0}$ and $J_{\rm g0}$ are the nominal values of $B_{\rm ls}$, $J_{\rm r}$ and $J_{\rm g}$, respectively. Then, rewrite system (10) as

$$\ddot{e} = \Psi + m_0T_{\rm em} - \ddot{\omega_{\rm r}}^* \tag{12}$$

When the output $\omega_{\rm r}$ is known, the states and perturbation of system can be estimated by a designed high-gain observer (HGO) proposed in [38].

$$\begin{cases}\dot{\hat{\omega}}_{\rm r} &= \hat{\omega}_{\rm r} + h_1(\omega_{\rm r} - \hat{\omega}_{\rm r}) \\ \dot{\hat{\omega}}_{\rm r} &= \hat{\Psi} + h_2(\omega_{\rm r} - \hat{\omega}_{\rm r}) + m_0T_{\rm em} \\ \dot{\hat{\Psi}} &= h_3(\omega_{\rm r} - \hat{\omega}_{\rm r}),\end{cases} \tag{13}$$

where, $\hat{\omega}_\mathrm{r}$, $\hat{\dot{\omega}}_\mathrm{r}$ and $\hat{\Psi}$ are the estimations of ω_r, $\dot{\omega}_\mathrm{r}$ and Ψ, respectively. h_i, $i = 1, 2, 3$ is the observer gain, which is designed as

$$h_i = \frac{\xi_i}{\epsilon^i} \tag{14}$$

where, ϵ is within (0,1). The parameters ξ_i are selected to make the roots of

$$s^3 + \xi_1 s^2 + \xi_2 s + \xi_3 = 0 \tag{15}$$

are on the open left-half complex plane.

3.2. Design of AAFT-MPPTC

When the actual perturbation Ψ is compensated by the perturbation estimation $\hat{\Psi}$, the control input T_em is expressed as follows

$$T_\mathrm{em} = m_0^{-1}(-\hat{\Psi} + v) \tag{16}$$

where, v is defined as

$$v = \ddot{\omega}_\mathrm{r}{}^* + k_\mathrm{p}(\omega_\mathrm{r}^* - \omega_\mathrm{r}) + k_\mathrm{i}(\dot{\omega}_\mathrm{r}{}^* - \hat{\dot{\omega}}_\mathrm{r}) \tag{17}$$

Then, the final control law represented by generator inertia, rotor inertia, low-speed shaft stiffness and rotor speed, is given as follows

$$T_\mathrm{em} = -\frac{J_\mathrm{r0}J_\mathrm{g0}N_\mathrm{g}}{B_\mathrm{ls0}}[k_\mathrm{p}(\omega_\mathrm{r}^* - \omega_\mathrm{r}) + k_\mathrm{i}(\dot{\omega}_\mathrm{r}{}^* - \hat{\dot{\omega}}_\mathrm{r}) + \ddot{\omega}_\mathrm{r}{}^* - \hat{\Psi}] \tag{18}$$

Note that only nominal parameter values of J_r0, J_g0 and B_ls0, and measurement of ω_r are required in the controller design.

The principle of proposed AAFT-MPPTC for the VSWT system has been clearly illustrated through a block diagram shown in Fig. 2.

3.3. Stability Analysis of VSWT Closed-Loop System

The stability of closed-loop VSWT system with the proposed AAFT-MPPTC is proved as follows.

Firstly, to obtain the tracking error and estimation error systems, the estimation errors are defined as $\zeta_1 = \omega_\mathrm{r} - \hat{\omega}_\mathrm{r}$, $\zeta_2 = \dot{\omega}_\mathrm{r} - \hat{\dot{\omega}}_\mathrm{r}$ and $\zeta_3 = \Psi - \hat{\Psi}$. The following estimation error system can be obtained by combining (13) and (14).

$$\dot{\zeta}_i = G_i\zeta_i + \varrho_i \tag{19}$$

where

$$\zeta_i = \begin{bmatrix} \zeta_1 \\ \zeta_2 \\ \zeta_3 \end{bmatrix}, \qquad \varrho_i = \begin{bmatrix} 0 \\ 0 \\ \Psi \end{bmatrix}, \tag{20}$$

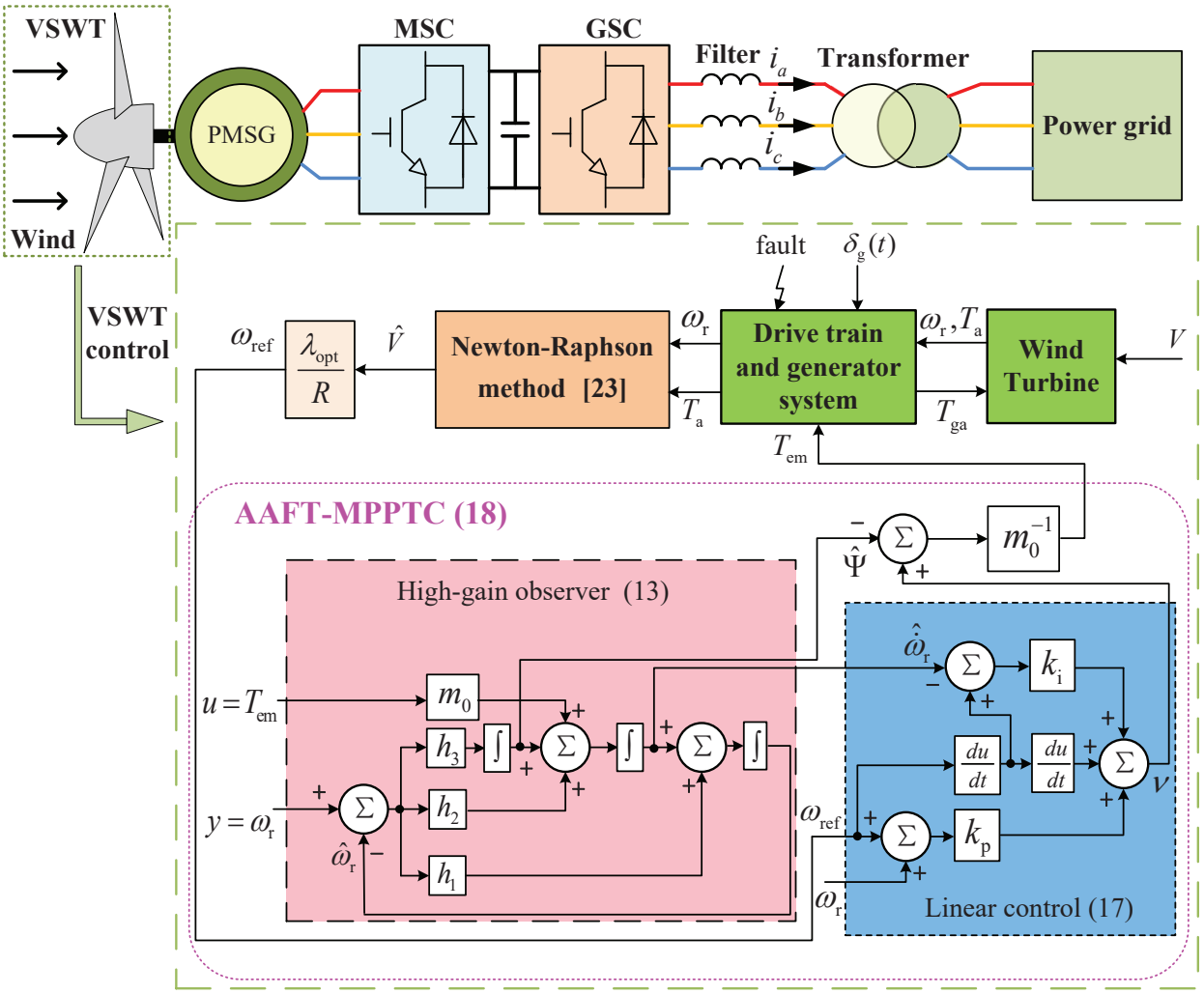

Figure 2: The AAFT-MPPTC control scheme for VSWT system

$$G_i = \begin{bmatrix} -h_1 & 1 & 0 \\ -h_2 & 0 & 1 \\ -h_3 & 0 & 0 \end{bmatrix} \tag{21}$$

Define the tracking errors as $\varepsilon_1 = \omega_{\mathrm{r}}^* - \omega_{\mathrm{r}}$ and $\varepsilon_2 = \dot{\omega}_{\mathrm{r}}^* - \dot{\omega}_{\mathrm{r}}$. Meanwhile, it can be obtained from (12), (16) and (17) that

$$\dot{\varepsilon}_2 = -[k_{\mathrm{p}}(\varepsilon_1 + \zeta_1) + k_{\mathrm{i}}(\varepsilon_2 + \zeta_2) + \zeta_3] \tag{22}$$

Consequently, the tracking error system can be represented as

$$\dot{\varepsilon}_i = \beta_i \varepsilon_i + \vartheta_i \tag{23}$$

where

$$\varepsilon_i = \begin{bmatrix} \varepsilon_1 \\ \varepsilon_2 \end{bmatrix}, \qquad \vartheta_i = \begin{bmatrix} 0 \\ -\xi \end{bmatrix}, \tag{24}$$

$$\beta_i = \begin{bmatrix} 0 & 1 \\ -k_\mathrm{p} & -k_\mathrm{i} \end{bmatrix} \tag{25}$$

with $\alpha = k_\mathrm{p}\zeta_1 + k_\mathrm{i}\zeta_2 + \zeta_3$ being the lumped estimation error.

Transform the stability analysis of the VSWT closed-loop control system into globally uniformly ultimately bounded.

Theorem 1. The proposed AAFT-MPPTC system of VSWT (18) is considered. When the actual perturbation Ψ (11) satisfies

$$\|\Psi\| \leq \theta_1 \tag{26}$$

then the tracking error system (23) and estimation error system (19) are, i.e.,

$$\|\zeta_i(t)\| \leq 2\theta_1\|Q_1\|, \|\varepsilon_i(t)\| \leq 4\theta_1\|K_i\|\|Q_1\|\|Q_2\|, \forall t \geq T \tag{27}$$

where Q_i, $i = 1, 2$ are the feasible solutions of Riccati equations $G_i^\mathrm{T}Q_1 + Q_1G_i = -I$ and $\beta_i^\mathrm{T}Q_2 + Q_2\beta_i = -I$, respectively; and $\|K_i\|$ is a constant related to k_p and k_i.

Proof. The following Lyapunov function is considered for estimation error system (19),

$$V_{i1}(\zeta_i) = \zeta_i^\mathrm{T}Q_1\zeta_i \tag{28}$$

The SPO gains used in (13) are determined by satisfying the requirement of (15). Calculate the derivative of $P_{i1}(\zeta_i)$ along (19) solution and use (26) to yield

$$\begin{aligned} \dot{P}_{i1}(\zeta_i) &= \zeta_i^\mathrm{T}(G_i^\mathrm{T}Q_1 + Q_1G_i)\zeta_i + \varrho_i^\mathrm{T}Q_1\zeta_i + \zeta_i^\mathrm{T}Q_1\varrho_i \\ &\leq -\|\zeta_i\|^2 + 2\|\zeta_i\| \cdot \|\varrho_i\| \cdot \|Q_1\| \\ &\leq -\|\zeta_i\|(\|\zeta_i\| - 2\theta_1\|Q_1\|) \end{aligned} \tag{29}$$

Then, when $\|\zeta_i\| \geq 2\theta_1\|Q_1\|$, $\dot{P}_{i1}(\zeta_i) \leq 0$. Therefore, it exists $T_1 > 0$, which can lead to

$$\|\zeta_i(t)\| \leq \theta_2 = 2\theta_1\|Q_1\|, \forall t \geq T_1 \tag{30}$$

In (23), $\|\varpi_i\| \leq \|K_i\|\theta_2$ with $\|K_i\|$ based on $\|\zeta_i(t)\| \leq \theta_2$ can be found. The Lyapunov function $P_{i2}(\varepsilon_i) = \varepsilon_i^\mathrm{T}Q_2\varepsilon_i$ is considered. Similarly, it can be proved that there is an instant, T_1,

$$\|\varepsilon_i(t)\| \leq 2\|K_i\|\theta_2\|Q_2\| \leq 4\theta_1\|K_i\|\|Q_1\|\|Q_2\|, \forall t \geq \bar{T}_1 \tag{31}$$

Using (30) and (31) and setting $T = \max\{T_1, \bar{T}_1\}$ lead to (27).

In addition, if Ψ and its derivative are locally Lipschitz in their arguments, it can ensure the exponential convergence of closed-loop tracking error and estimation error [39].

$$\lim_{t\to\infty} \zeta_i(t) = 0 \quad \text{and} \quad \lim_{t\to\infty} \varepsilon_i(t) = 0 \tag{32}$$

When the state ω_r and its derivatives are stable under the AAFT-MPPTC, it is proved that the error system converges to zero in (32). It ensures that the extended states defined in (11) including parameter uncertainties and unknown disturbances caused by disturbance torque and generator actuator failure can be tracked by the estimated perturbations, and the control input in (16) can be compensated.

Table 1: Parameters of the VSWT in simulation studies

Parameters	Values	Units
Blade radius R	21.65	m
Air density ρ	1.29	kg/m^3
Optimal blade tip ratio λ_{opt}	6.325	
Maximum power coefficient C_{pmax}	0.4382	
Inertia of rotor J_r	325,000	kg.m^2
Inertia of generator J_g	34.4	kg.m^2
Damping of low-speed shaft K_s	9,500	N.m/rad/s
Stiffness of low-speed shaft D_s	269,100	N.m/rad
External damping of rotor K_r	27.36	N.m/rad/s
External damping of generator K_g	0.2	N.m/rad/s
Gearbox ratio N_g	43.165	

Table 2: Parameters of AAFT-MPPTC scheme in simulation studies

Parameters of the AAFT-MPPTC (18)	
Gains of observer (13)	$\xi_1 = 2.7 \times 10^2$, $\xi_2 = 2.43 \times 10^4$, $\xi_3 = 7.29 \times 10^5$, $\epsilon = 0.02$
Gains of linear controller (17)	$k_\mathrm{p} = 25$, $k_\mathrm{i} = 10$

4. Simulation Studies

To verify the performance of proposed AAFT-MPPTC, the PI, MPPT mentioned in [35] and NSSF-MPPT proposed in [35] are employed for comparisons. The specifications of the VSWT are listed in Table 1 [7, 35]. In addition, the parameters of the proposed AAFT-MPPTC are designed based on pole-placement, as shown in Table 2. The advantages of AAFT-MPPTC are verified by simulation tests under four different scenarios: time-varying wind speed,

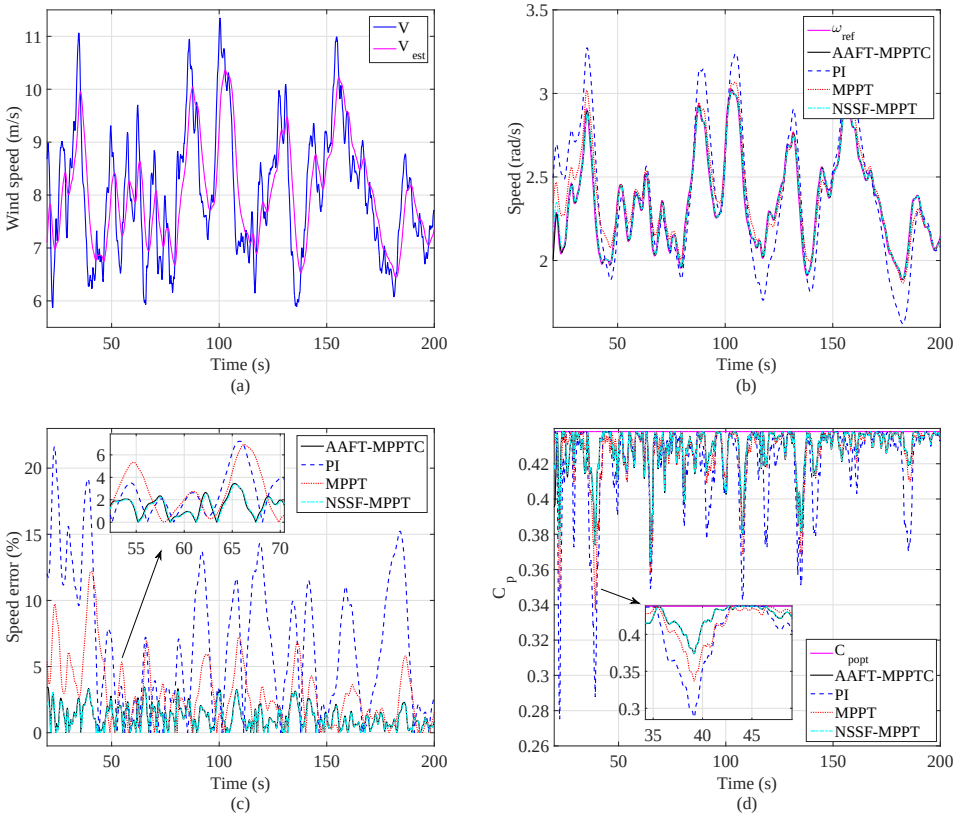

Figure 3: Response curves under time-varying wind speed. (a) Wind speed V; (b) rotor speed ω_{r}; (c) relative error of ω_{r}; (d) power coefficient C_{p}.

parameter uncertainties, generator actuator failure at constant wind speed, and simultaneous existence of generator actuator failure and disturbance torque at constant wind speed. In this paper, simulation tests are conducted by Matlab/Simulink.

4.1. Scenario I: Time-Varying Wind Speed

4.1.1. Comparisons of PI, MPPT, NSSF-MPPT and AAFT-MPPTC

The response curves of VSWT to time-varying wind speed are shown in Figs. 3-8. In Fig. 3 (a), although the estimation error exists, the actual wind speed with high turbulency can still be well estimated. Figs. 3 (b) and (c) show that both the AAFT-MPPTC and NSSF-MPPT obtain better tracking performances of the rotor speed ω_{r} than the PI and NSSF-MPPT controllers, and the worst tracking performances are obtained by the PI. It is because that the global optimal performance can be provided by the NSSF-MPPT and AAFT-MPPTC under time-varying operation points, which cannot be provided by the PI designed based on one operation point. It is worth noting that the NSSF-MPPT requires full state measurements and detailed system model. When the rotor speed ω_{r} cannot track its optimal reference ω_{ref} well, the maximum power coefficient C_{popt} cannot be ensured, as shown in Fig. 3 (d). In Fig. 4, the

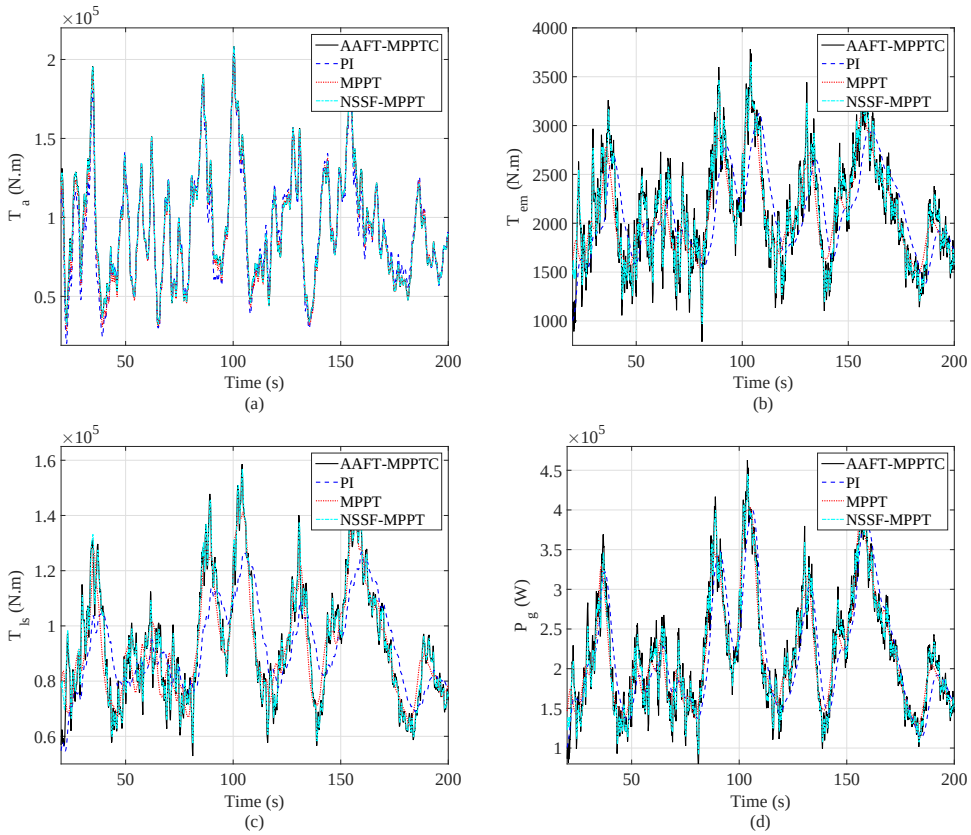

Figure 4: Response curves under time-varying wind speed. (a) Aerodynamic torque T_{a}; (b) generator torque T_{em}; (c) low-speed shaft torque T_{ls}; (d) generator power P_{g}.

responses of aerodynamic torque T_{r}, generator torque T_{em}, low-speed shaft torque T_{ls} and generator power P_{g} have been given.

The comparison between the actual perturbation Ψ and its estimated value is shown in Fig. 5. Although there is estimation error, it provides satisfactory estimation performances in most cases, as shown in Fig. 5(b). The estimation error is generated under the rapidly changing disturbance, because the observer needs a certain time for estimation. It can be found from Fig. 6 that, both the NSSF-MPPT and AAFT-MPPTC achieve much better control performance than PI and MPPT in terms of the integral of the time multiplied by the absolute error (ITAE) and maximum regulation error (MRE).

4.1.2. Comparisons of Controllers Based on Different Observers

For the comparisons of controllers based on different observers, NAC based on sliding-mode perturbation observer (SMPO-NAC) in [39] and active disturbance rejection control based MPPT (ADRC-MPPT) [40] are employed to compare with the proposed AAFT-MPPTC in this subsection. Fig. 7 shows that the SMPO-NAC, ADRC-MPPT and AAFT-MPPTC almost achieve the same dynamic performances. Meanwhile, the similar control performances in

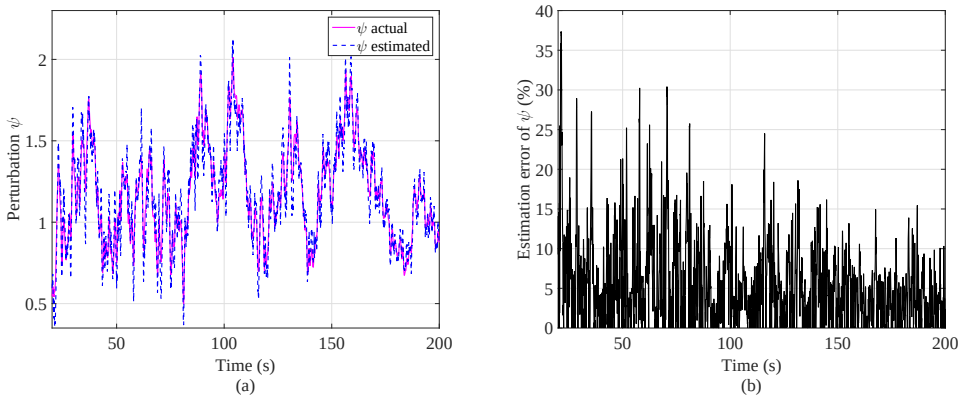

Figure 5: Perturbation estimation. (a) Perturbation Ψ; (b) relative error of Ψ.

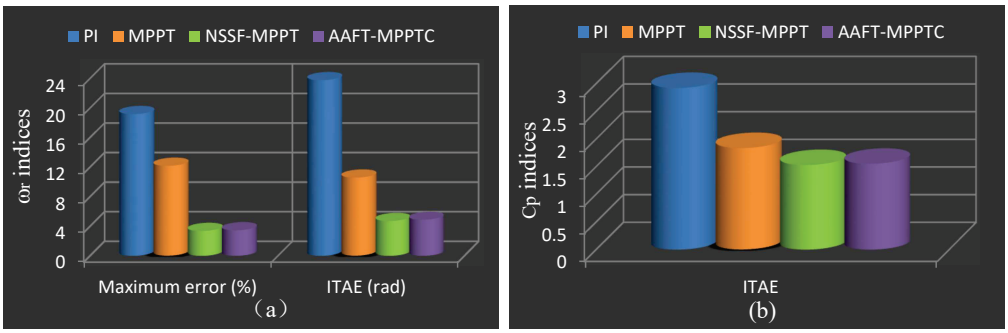

Figure 6: Comparisons of performance indices in MRE and ITAE at time-varying wind speed. (a) ω_{r}; (b) C_{p}.

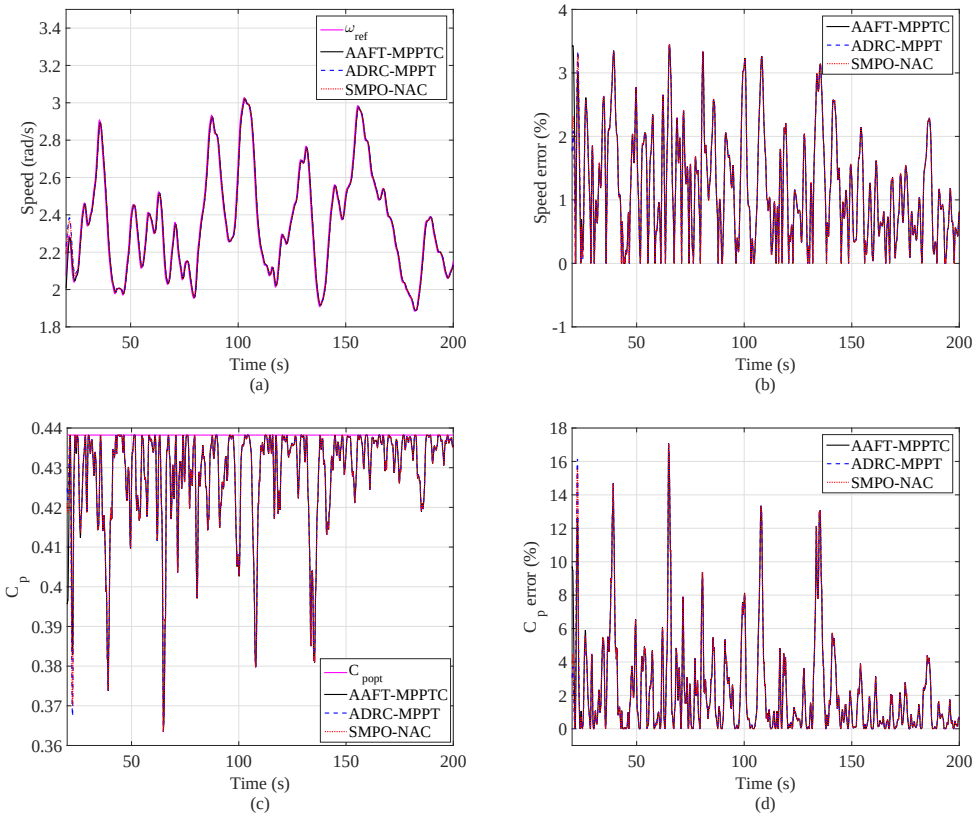

Figure 7: Responses curves of observer based controllers at time-varying wind speed. (a) Rotor speed ω_{r}; (b) relative error of ω_{r}; (c) power coefficient C_{p}; (d) relative error of C_{p}.

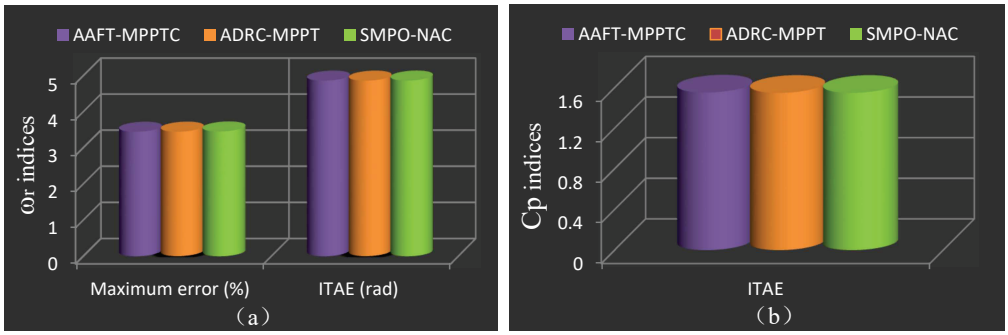

Figure 8: Comparisons of control performance indices in MRE and ITAE at time-varying wind speed. (a) ω_r; (b) C_p.

terms of the ITAE and MRE can be provided by these three controllers based on different observers, as shown in Fig. 8. Among them, the AAFT-MPPTC is simple in stability analysis, gain tuning and structure.

4.2. Scenario II: Parameter Uncertainties

With the change of operation time and environment, it is difficult for a VSWT to keep the system parameters consistent with their nominal values. Therefore, the influence of system parameter uncertainties on the control system needs to be tested. Due to page limit, only the simulation case of rotor inertia J_r mismatch is tested in this subsection, which varies from 0.8 p.u. to 1.2 p.u.. The wind speed employed in this test case is the same as that depicted in Fig. 3(a).

It can be found from Fig. 9(a) that, comparing with the PI and MPPT controllers, both the AAFT-MPPTC and NSSF-MPPT have much smaller variations in the maximum error of the rotor speed ω_r under the change of J_r. The variation of the maximum error for the rotor speed ω_r under the NSSF-MPPT is more obvious than that obtained under the AAFT-MPPTC. In Fig. 9(b), the change of J_r hardly affects the maximum error of the rotor speed ω_r under the observer-based controllers. It means the control performance can be affected by the parameter variations under the PI, MPPT and NSSF-MPPT. The AAFT-MPPTC can provide higher robustness against parameter uncertainties than the PI, MPPT and NSSF-MPPT.

4.3. Scenario III: Generator Actuator Failure at Constant Wind Speed

In this test scenario, the VSWT operates at a constant wind speed 8 m/s for 100 s with two operation stages. In the first stage, the VSWT operates for 40 s without failure or disturbance torque, then the health indicator of the generator actuator suddenly reduces from 1 to 0.6 in the second stage, which can be expressed as

$$\rho(t) = \begin{cases} 1, & 0 \le t < 40 \\ 0.6, & t \ge 40 \end{cases} \tag{33}$$

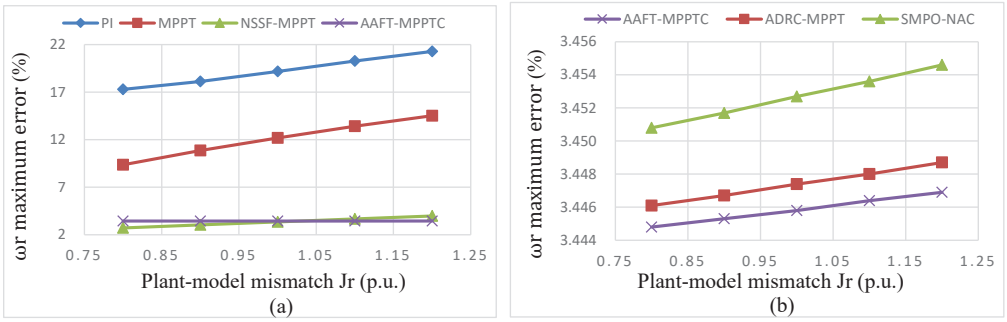

Figure 9: Comparisons of performance indices in MRE under rotor inertia variation.

4.3.1. Comparisons of PI, MPPT, NSSF-MPPT and AAFT-MPPTC

It can be seen from Figs. 10 and 11 that, all of the four controllers can achieve satisfactory performances in the first stage. However, the performances of the PI, MPPT and NSSF-MPPT all significantly degrade in the second stage except the AAFT-MPPTC. Not only that, the rotor speed ω_r exists steady state errors under both the NSSF-MPPT and MPPT, as shown in Figs. 10(a) and (b). It means that the steady-state error will not be eliminated if the generator actuator failure is not resolved. During the VSWT operation, the NSSF-MPPT controller cannot recognize the generator actuator failure without FDI technologies. Hence, the health indicator of the generator actuator $\rho(t)$ in (10) is considered to be 1, which leads to the steady state error of the rotor speed ω_r under the NSSF-MPPT control. In the MPPT controller design, the generator torque T_{em} is closely related to the generator speed ω_g, which is given by (16) in [35]. Hence, the control performance of MPPT controller may deteriorate if the information of generator torque is inaccurate, such as unknown generator actuator failure. Compared with the NSSF-MPPT and MPPT, although the PI has tracking error of the rotor speed ω_r, the steady state of the ω_r can be recovered in approximately 60 s. According to (6), when the ω_r has a deviation with its optimal reference, the optimal TSR cannot be achieved. Therefore, the C_p cannot reach its maximum value, as shown in Figs. 10(b) and (c). The maximum and smallest errors of the C_p are obtained by the MPPT and AAFT-MPPTC controllers, respectively.

It can be seen from Fig. 11 that, the PI, MPPT and NSSF-MPPT all cannot always keep consistent responses of the T_a, T_{em}, P_a and P_g under generator actuator failure. The proposed AAFT-MPPTC can always provide satisfactory performance. Although the generator actuator failure occurs, the perturbation caused by the generator actuator failure can be compensated in real-time by estimated perturbation, as shown in Fig. 12. Hence, the response of the generator torque T_{em} is almost unaffected by the generator actuator failure. Because the change of health indication is set as step change in this test case, it is difficult for the designed observer to provide accurate estimation of the actual perturbation immediately. Therefore, there is a large estimation error at the moment of occurring generator actuator failure, but the error will be quickly eliminated, as shown in Fig. 12.

The performances of the PI, MPPT, NSSF-MPPT and AAFT-MPPTC controllers represented by the ITAE and MRE of ω_r are shown in Fig. 13. The results show that the proposed AAFT-MPPTC is most insensitive to the

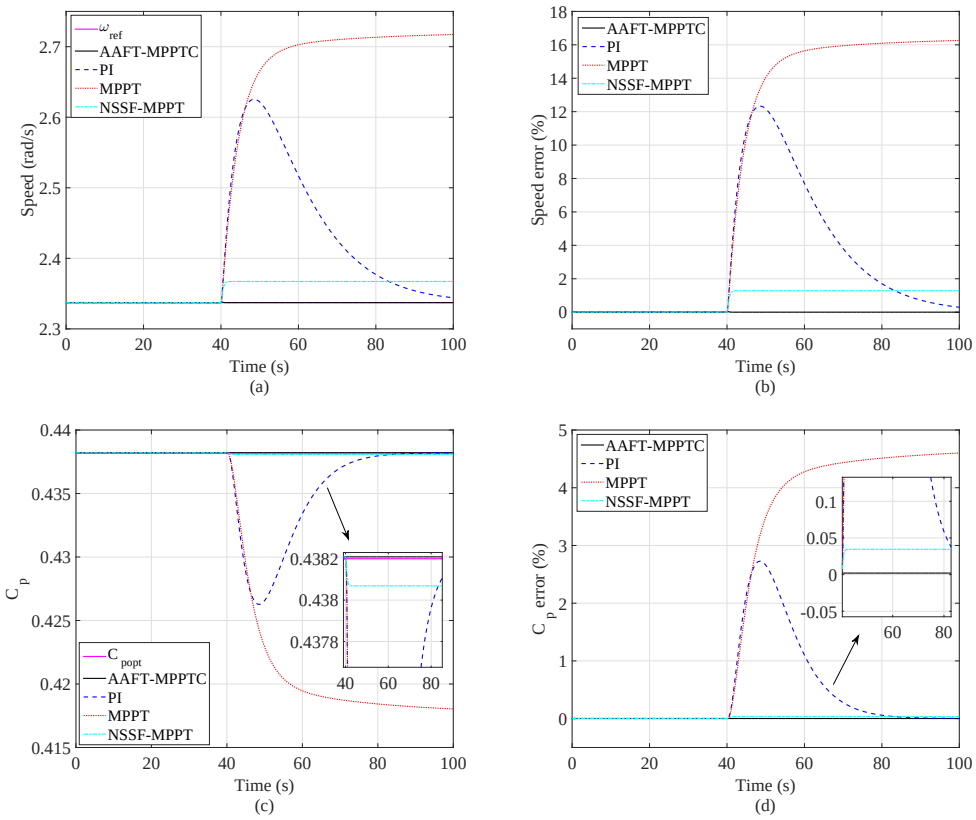

Figure 10: Response curves under generator actuator failure. (a) Rotor speed ω_{r}; (b) relative error of ω_{r}; (c) power coefficient C_{p}; (d) relative error of C_{p}.

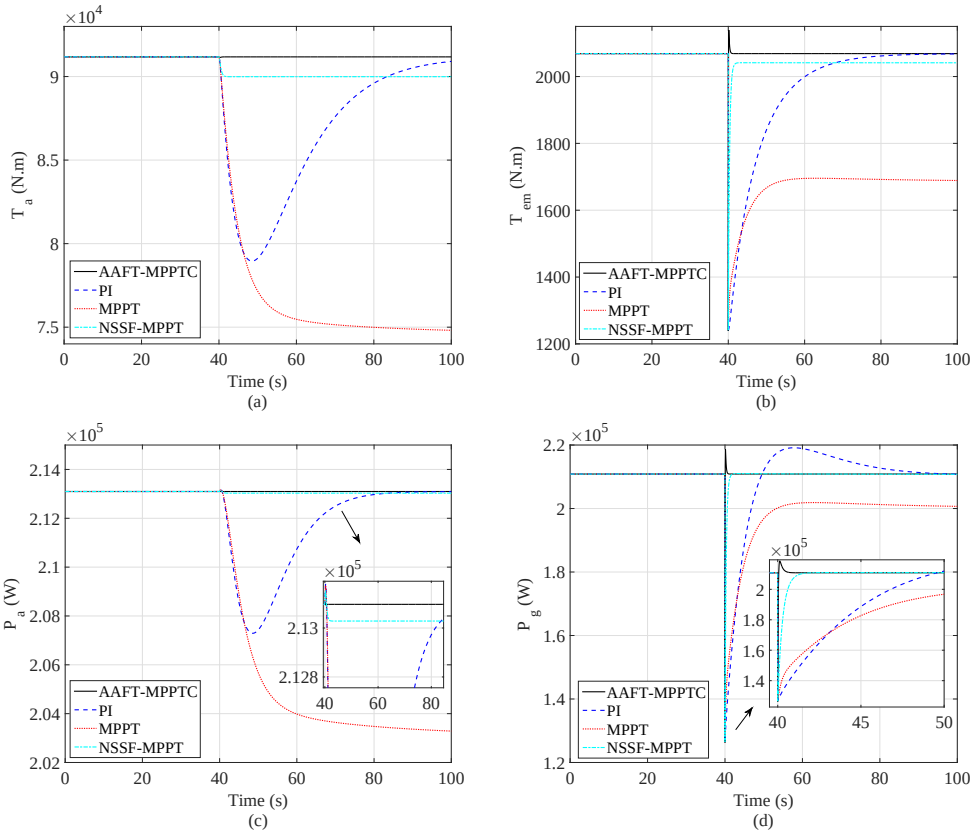

Figure 11: Response curves under generator actuator failure. (a) Aerodynamic torque T_{a}; (b) generator torque T_{em}; (c) aerodynamic power P_{a}; (d) generator power P_{g}.

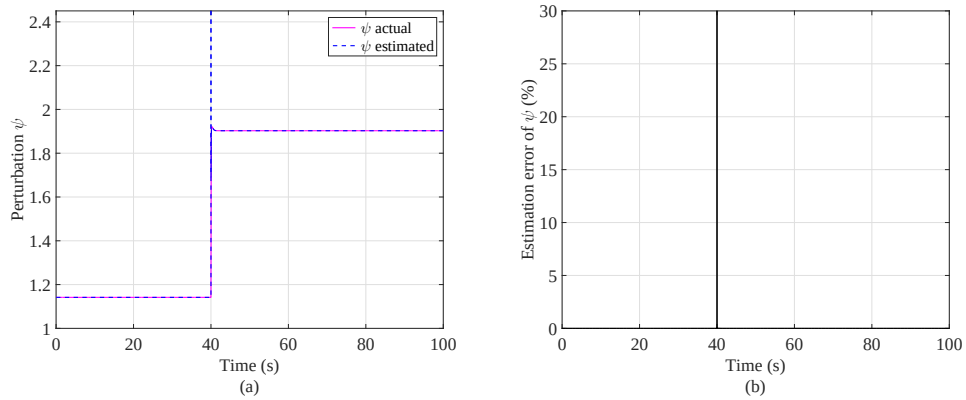

Figure 12: Perturbation estimation. (a) Perturbation Ψ; (b) relative error of Ψ.

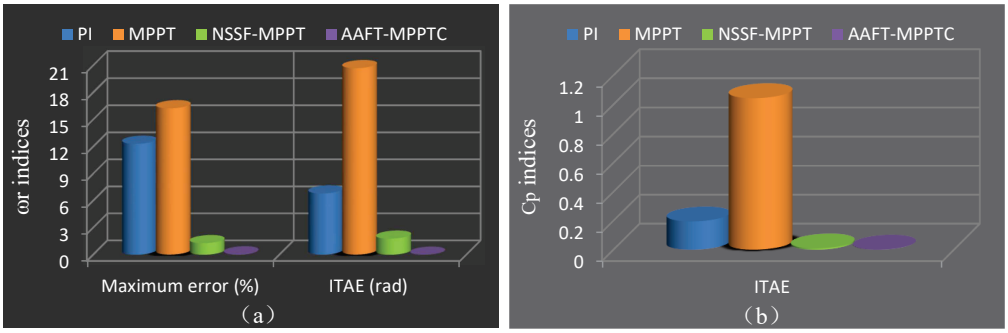

Figure 13: Comparisons of performance indices in MRE and ITAE under generator actuator failure. (a) ω_r; (b) C_p.

generator actuator failure.

4.3.2. Comparisons of Controllers Based on Different Observers

The comparisons of control performance among the AAFT-MPPTC, ADRC-MPPT and SMPO-NAC under generator actuator failure are shown in Fig. 14. All these three controllers provide high robustness against generator actuator failure. The AAFT-MPPTC achieves a little better tracking performance than the other two controllers. In Fig. 15, it can be found that the AAFT-MPPTC provides the highest robustness against generator actuator failure among these three controllers.

4.4. Scenario IV: Generator Actuator Failure and Disturbance Torque at Constant Wind Speed

To further verify the effectiveness of the proposed AAFT-MPPTC method, both the disturbance torque and generator actuator failure are considered in this test scenario. The wind speed maintains at 8 m/s for 100 s. The disturbance torque $\delta_g(t)$ and health indicator $\rho(t)$ are shown in Figs. 16(a) and (b), respectively.

4.4.1. Comparisons of PI, MPPT, NSSF-MPPT and AAFT-MPPTC

In the first 60 s of simulation test, only the disturbance torque $\delta_g(t)$ is applied. The rotor speed ω_r is with big deviation from its optimal reference ω_{ref} under both the PI and MPPT controllers, as shown in Figs. 16(c) and (d). It is because that the PI controller designed based on one operation point cannot provide consistent response under the varying operation points caused by the disturbance torque $\delta_g(t)$. In the MPPT controller design, the disturbance has not been considered. The disturbance torque $\delta_g(t)$ affects the tracking performance of ω_r. Comparing with the PI and MPPT controllers, the NSSF-MPPT controller provides much smaller tracking error, but the steady state error exists. Note that the disturbance torque $\delta_g(t)$ is unknown in the NSSF-MPPT controller, which is considered to be 0 N.m. Hence, the NSSF-MPPT controller cannot provide consistent performance when the disturbance torque $\delta_g(t)$ occurs.

When both the generator actuator fault and disturbance torque $\delta_g(t)$ are applied (from 60 s to 70 s), the PI, MPPT and NSSF-MPPT controllers all provide increased tracking errors of the rotor speed ω_r, as shown in Figs. 16(c) and

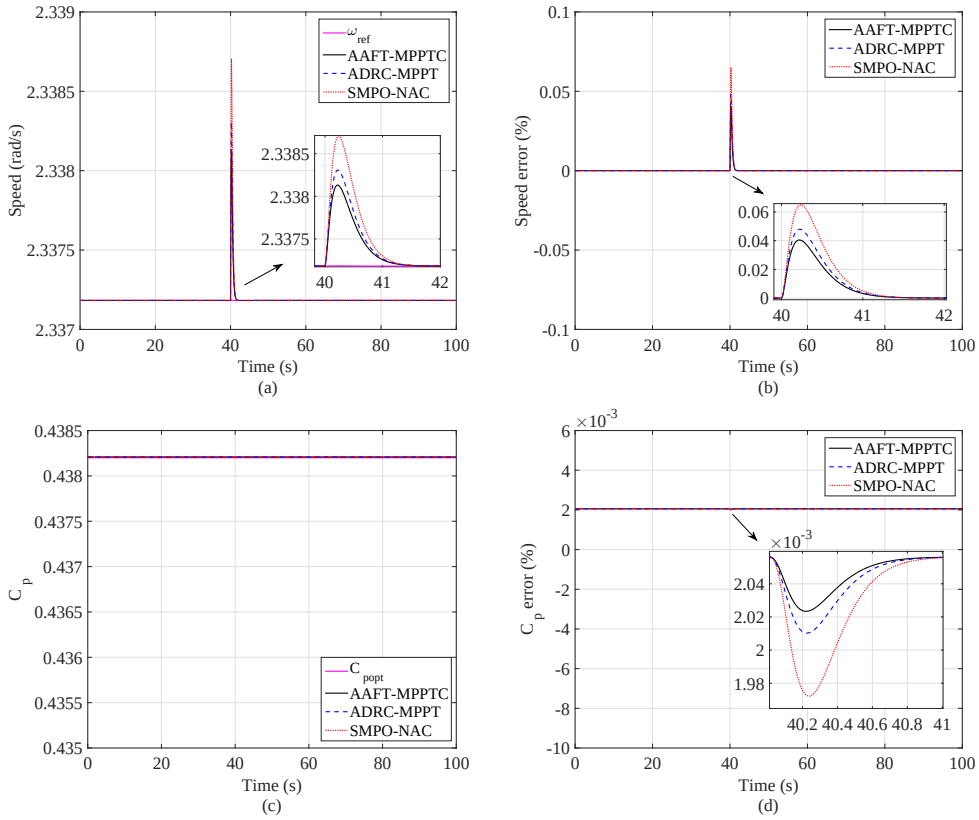

Figure 14: Response curves of observer based controllers under generator actuator failure. (a) Rotor speed ω_r; (b) relative error of ω_r; (c) power coefficient C_p; (d) relative error of C_p.

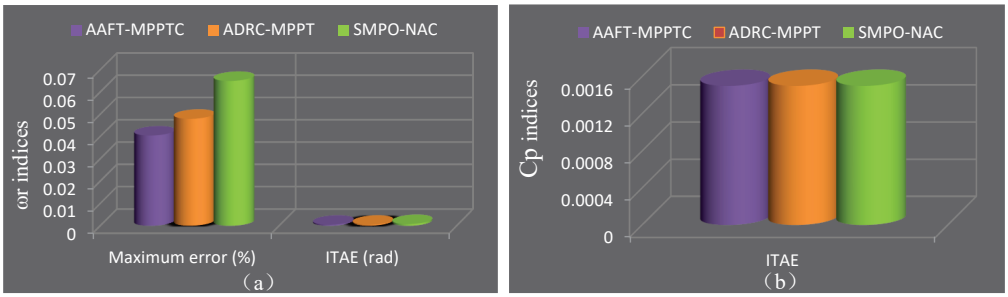

Figure 15: Comparisons of performance indices in MRE and ITAE under generator actuator failure. (a) ω_r; (b) C_p.

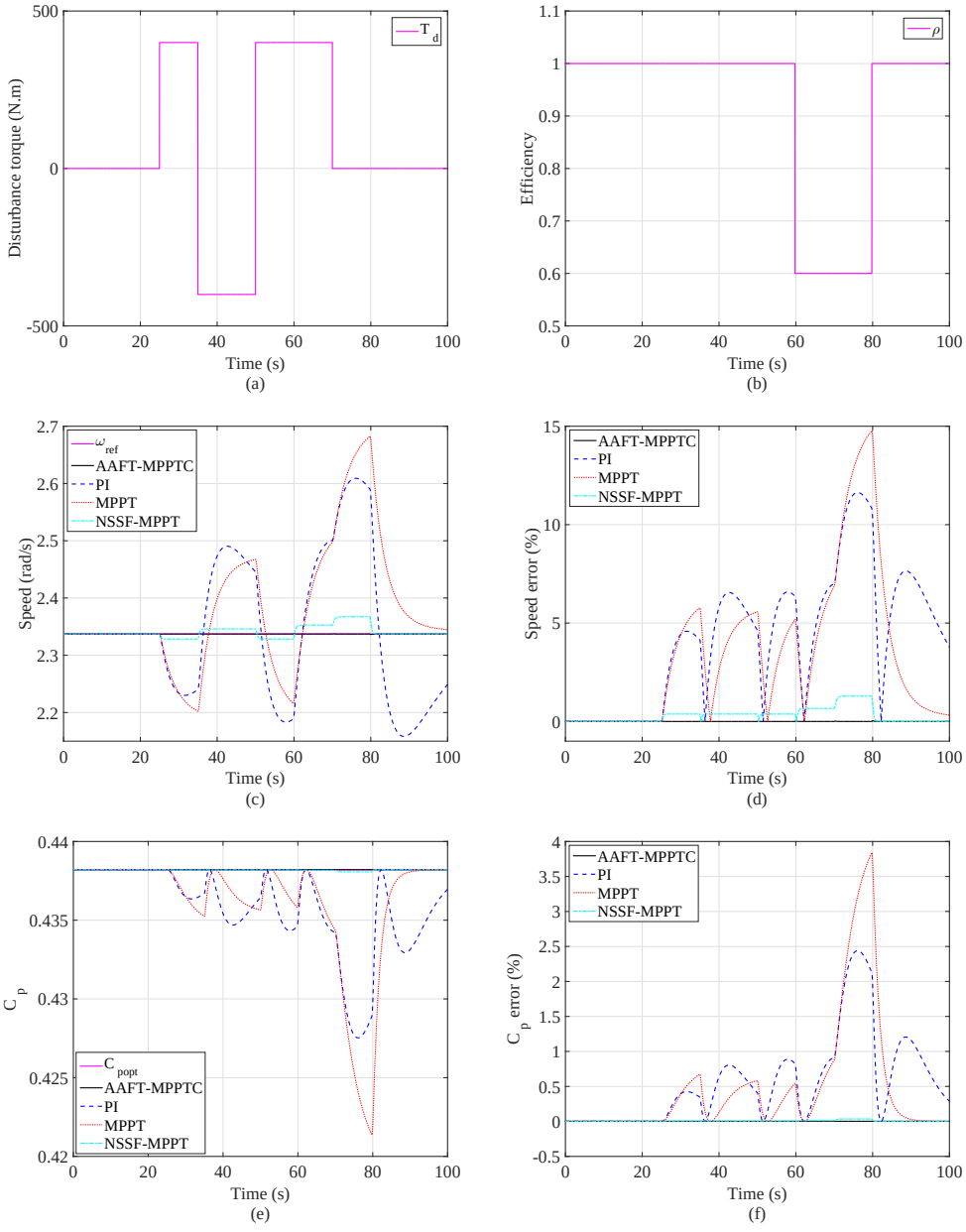

Figure 16: Response curves under generator actuator fault and disturbance torque. (a) Health indicator $\rho(t)$; (b) disturbance torque $\delta_{\mathrm{g}}(t)$; (c) rotor speed ω_{r}; (d) relative error of ω_{r}; (e) power coefficient C_{p}; (f) relative error of C_{p}.

(d). From 70 s to 80 s, only generator actuator failure is considered in the simulation test. Figs. 16(c) and (d) show that the tracking error of the rotor speed ω_r is further increased under the PI, MPPT and NSSF-MPPT control. The dynamic performance is still affected by the generator actuator failure. In the last 20 s of simulation test, the VSWT recovers to normal operation. The rotor speed ω_r immediately reaches its optimal reference ω_{ref} under the NSSF-MPPT control. However, both the PI and MPPT need more than 20 s for recovering to its optimal reference. Note that among these four controllers, the AAFT-MPPTC always provides satisfactory performance with much smaller tracking error, which is almost unaffected by the disturbance torque $\delta_g(t)$ and generator actuator failure.

The power coefficient C_p deviates from its maximum value C_{popt} due to the tracking error of the ω_r, as shown in Figs. 16 (e) and (f). It can be found from Fig. 17(a) that compared with the PI and MPPT controllers, the dynamic response of the T_a under the NSSF-MPPT control is less affected by the generator actuator failure and disturbance torque $\delta_g(t)$. The PI, MPPT and NSSF-MPPT controllers all lack the real-time compensation technology of the AAFT-MPPTC for the perturbation caused by the generator actuator failure and disturbance torque $\delta_g(t)$, which leads to the failure of the generator torque T_{em} to maintain a consistent dynamic response, as shown in Fig. 17(b). The responses of the T_{ls} and P_g have shown in Figs. 17(c) and (d), respectively. The consistent dynamic responses of the system can be obtained by the proposed AAFT-MPPTC, which is inseparable from the satisfactory estimated performance provided by the designed observer. The perturbation caused by the generator actuator failure and disturbance torque $\delta_g(t)$ can be well estimated by the designed observer, except for the moment of step change, as shown in Fig. 18.

Fig. 19 shows the performances of the PI, MPPT, NSSF-MPPT and AAFT-MPPTC control methods through ITAE and MRE of ω_r. The proposed AAFT-MPPTC provides the highest robustness against the disturbance torque and generator actuator failure.

4.4.2. Comparisons of Controllers Based on Different Observers

The comparisons of control performance among the SMPO-NAC, ADRC-MPPT and AAFT-MPPTC under the disturbance torque and generator actuator failure are shown in Fig. 20. These three controllers provide similar performance with quite small tracking error of rotor speed ω_r. Hence, the C_p is always around its maximum value C_{popt}. Among these three controllers, the AAFT-MPPTC is with smallest tracking error of the rotor speed ω_r and most insensitive to the disturbance torque and generator actuator failure, as shown in Figs. 20 and 21.

5. Conclusions

In this paper, an AAFT-MPPTC controller without employing FDI technologies has been proposed to provide high dynamic performance for a two-mass model based WT and high robustness against generator actuator failure, parameter uncertainties and disturbance torque. In the proposed control strategy, to compensate the perturbations caused by disturbance torque, parameter uncertainties, unknown nonlinearities and generator actuator failure, an H-GO has been designed to estimate the real perturbation in real-time. After the compensation, the VSWT system is fully linearized with few system state measurements by adopting a linear output feedback control law. In addition,

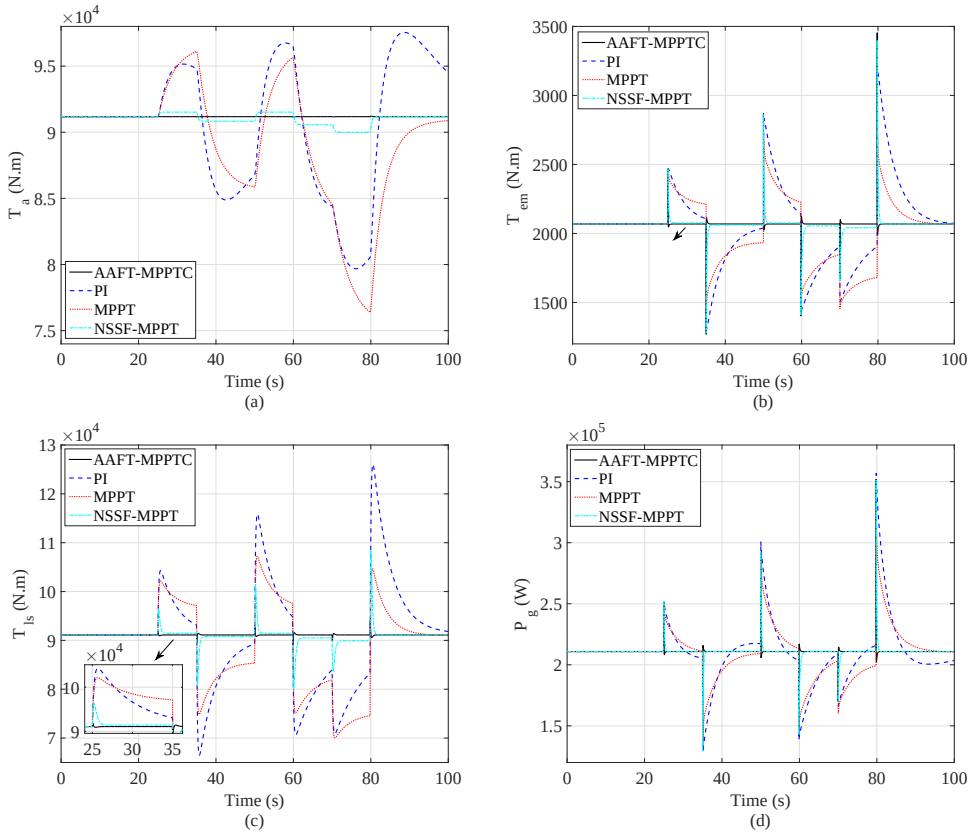

Figure 17: Response curves under generator actuator failure and disturbance torque. (a) Aerodynamic torque T_{a}; (b) generator torque T_{em}; (c) low-speed shaft torque T_{ls}; (d) generator power P_{g}.

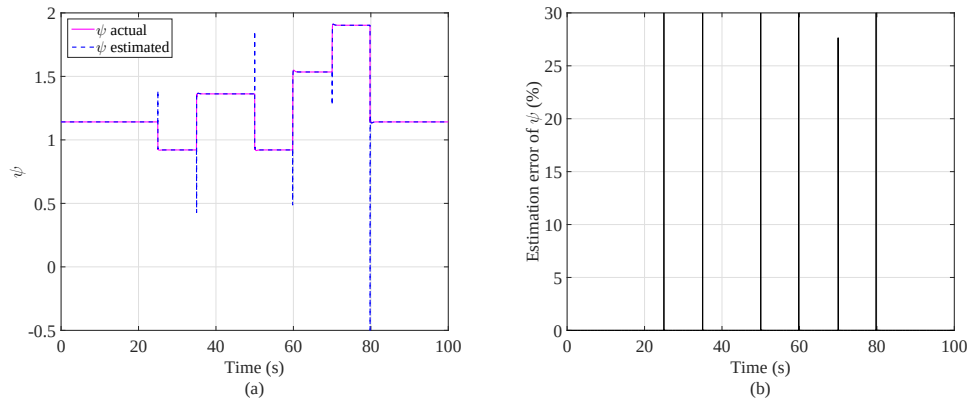

Figure 18: Perturbation estimation. (a) Perturbation Ψ; (b) relative error of Ψ.

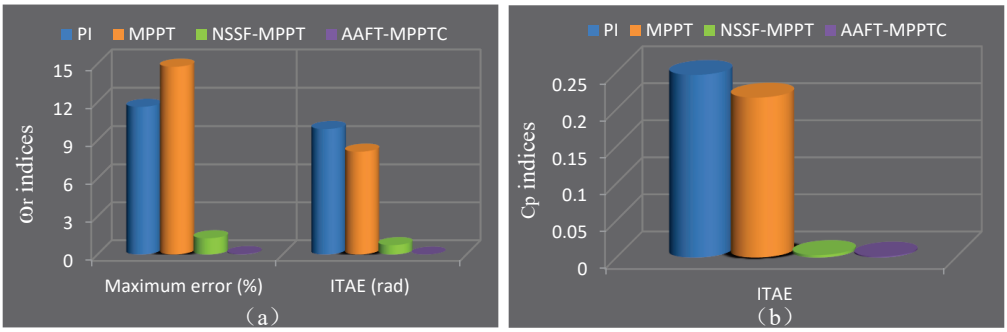

Figure 19: Comparisons of performance indices in MRE and ITAE under generator actuator failure and disturbance torque. (a) ω_r; (b) C_p.

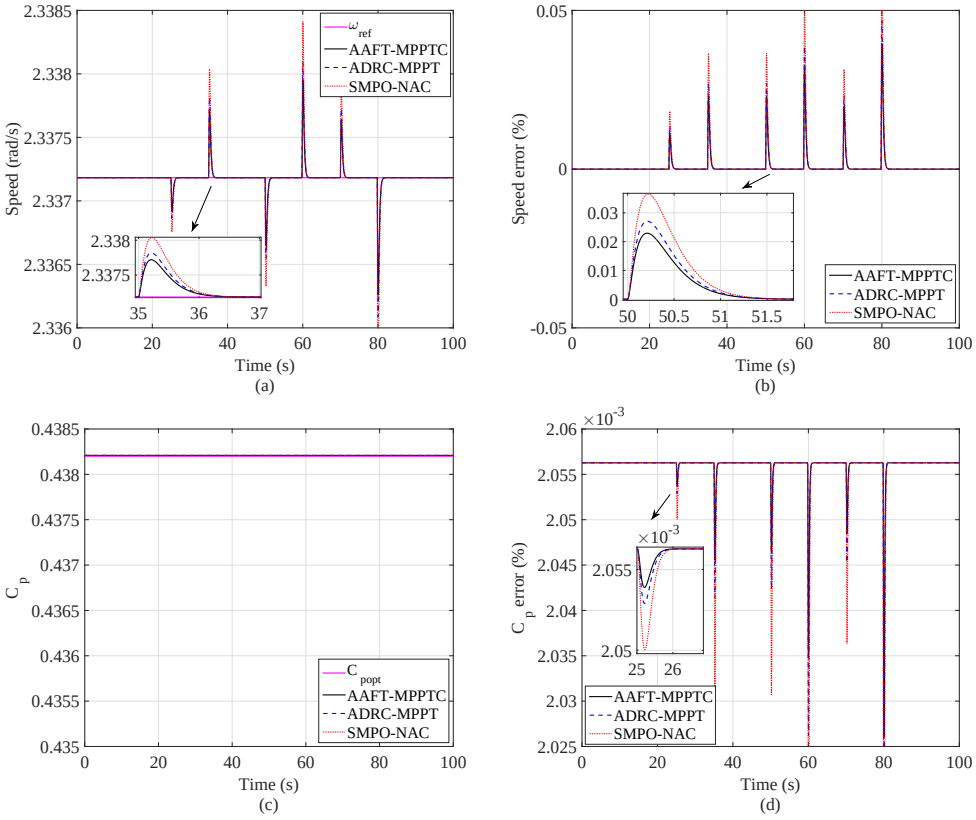

Figure 20: Response curves of observer based controllers under generator actuator failure and disturbance torque. (a) Rotor speed ω_r; (b) relative error of ω_r; (c) power coefficient C_p; (d) relative error of C_p

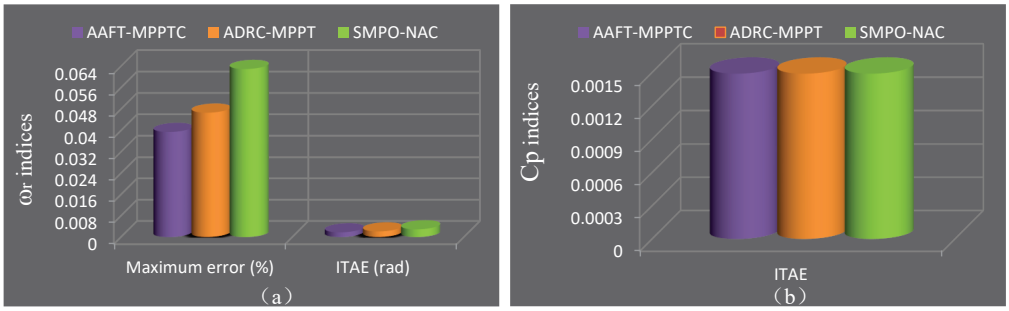

Figure 21: Comparisons of performance indices in MRE and ITAE under generator actuator failure and disturbance torque. (a) ω_{r}; (b) C_{p}.

the Newton-Rafson iterative method has been employed for wind speed estimation. Compared with the PI designed based on one operation point, and MPPT relying on the strict nonlinear relationship between the generator torque T_{em} and generator speed ω_{g}, and without considering the dynamic aspect of the wind and VSWT, the AAFT-MPPTC provides global optimal performance at time-varying wind speed. Especially, the AAFT-MPPTC achieves much better dynamic performances than these two controllers under the parameter uncertainties, generator actuator failure and disturbance torque. Although the NSSF-MPPT designed based on full state measurements and accurate system parameters achieves similar performance with the AAFT-MPPTC at time-varying wind speed, whose control performance is affected under parameter uncertainties, generator actuator failure and disturbance torque. Among these four controllers, the proposed AAFT-MPPTC always provides best dynamic performance and ensures highest robustness against parameter uncertainties, generator actuator failure and disturbance torque.

Further studies will focus on carrying the experimental test of the proposed method on a hardware prototype and investigating its potential to deal with MPPT control and asymmetrical voltage sags of the whole WPS.

Acknowledgements

This work is supported by the Natural Science Foundation of the Jiangsu Higher Education Institutions of China (Grant NO.19KJB470036), National Natural Science Foundation of China under Grant NO.62003292, and National Natural Science Foundation of China under Grant No.52022035.

[1] Badihi H, Jadidi S, Zhang YM, Pillay P, Rakheja S. Fault-tolerant cooperative control in a wind farm using adaptive control reconfiguration and control reallocation. IEEE Transactions on Sustainable Energy 2020;11(4):2119-2129.

[2] Badihi H, Zhang YM, Hong H. Wind turbine fault diagnosis and fault-tolerant torque load control against actuator faults. IEEE Transactions on Control Systems Technology 2015;23(4):1351-1372.

[3] Lin ZW, Chen ZY, Wu QW, Yang S, Meng HM. Coordinated pitch & torque control of large-scale wind turbine based on Pareto efficiency analysis. Energy 2018;147:812-825.

[4] Nayeh RF, Moradi H, Vossoughi G. Multivariable robust control of a horizontal wind turbine under various operating modes and uncertainties: a comparison on sliding mode and H_∞ control. International Journal of Electrical Power & Energy Systems 2020;115:105474.

[5] Huang C, Li FX, Jin ZQ. Maximum power point tracking strategy for large-scale wind generation systems considering wind turbine dynamics. IEEE Transactions on Industrial Electronics 2015;62(4):2530-2539.

[6] Yang B, Zhang XS, Yu T, Shu HC, Fang ZH. Grouped grey wolf optimizer for maximum power point tracking of doubly-fed induction generator based wind turbine. Energy Conversion and Management 2017;133:427-443.

[7] Wu AH, Zhao BH, Mao JF, Wu BW, Yu F. Adaptive active fault-tolerant MPPT control for wind power generation system under partial loss of actuator effectiveness. International Journal of Electrical Power & Energy Systems 2019;105:660-670.

[8] Li DY, Song YD, Gan ZX, Cai WC. Fault-tolerant optimal tip-speed-ratio tracking control of wind turbines subject to actuation failures. IEEE Transactions on Industrial Electronics 2015;62(12):7513-7523.

[9] Fathabadi H. Novel high efficient speed sensorless controller for maximum power extraction from wind energy conversion systems. Energy Conversion and Management 2016;123:392-401.

[10] Youssef AR, Ali AIM, Saeed MSR, Mohamed EEM. Advanced multi-sector P&O maximum power point tracking technique for wind energy conversion system. International Journal of Electrical Power & Energy Systems 2019;107:89-97.

[11] Karabacak M, Fernández-Ramírez LM, Kamal T, Kamal S. A new hill climbing maximum power tracking control for wind turbines with inertial effect compensation. IEEE Transactions on Industrial Electronics 2019;66(11):8545-8556.

[12] Wei C, Zhang Z, Qiao W, Qu LY. An adaptive network-based reinforcement learning method for MPPT control of PMSG wind energy conversion systems. IEEE Transactions on Power Electronics 2016;31(11):7837-7848.

[13] Yin MH, Li WJ, Chung CY, Zhou LJ, Chen ZY, Zhou Y. Optimal torque control based on effective tracking range for maximum power point tracking of wind turbines under varying wind conditions. IET Renewable Power Generation 2017;11(4):501-510.

[14] Zhang XL, Zhang YF, Hao SP, Wu L, Wei W. An improved maximum power point tracking method based on decreasing torque gain for large scale wind turbines at low wind sites. Electric Power Systems Research 2019;176:105942.

[15] Yang B, Yu T, Shu HC, Zhang YM, Chen J, Sang YY, Jiang L. Passivity-based sliding-mode control design for optimal power extraction of a PMSG based variable speed wind turbine. Renewable Energy 2018;119:577-589.

[16] Chen J, Yao W, Zhang CK, Ren YX, Jiang L. Design of robust MPPT controller for grid-connected PMSG-based wind turbine via perturbation observation based nonlinear adaptive control. Renewable Energy 2019;134:478-495.

[17] Mérida J, Aguilar LT, Dávila J. Analysis and synthesis of sliding mode control for large scale variable speed wind turbine for power optimization. Renewable Energy 2014;71:715-728.

[18] Golnary F, Moradi H. Design and comparison of quasi continuous sliding mode control with feedback linearization for a large scale wind turbine with wind speed estimation. Renewable Energy 2018;127:495-508.

[19] Song DR, Yang J, Cai ZL, Dong M, Su M, Wang YH. Wind estimation with a non-standard extended Kalman filter and its application on maximum power extraction for variable speed wind turbines. Applied Energy 2017;190:670-685.

[20] Mousa HHH, Youssef AR, Mohamed EEM. State of the art perturb and observe MPPT algorithms based wind energy conversion systems: A technology review. International Journal of Electrical Power & Energy Systems 2021;126:106598.

[21] Song DR, Yang YG, Zheng SY, Deng XF, Yang J, et al. New perspectives on maximum wind energy extraction of variable-speed wind turbines using previewed wind speeds. Energy Conversion and Management 2020;206:112496.

[22] Song DR, Liu JB, Yang YG, Yang J, Su M, Wang Y, et al. Maximum wind energy extraction of large-scale wind turbines using nonlinear model predictive control via Yin-Yang grey wolf optimization algorithm. Energy 2020;221:119866.

[23] Chen J, Lu Q, Chen LB, Duan XH, Yang BP, et al. Nonlinear maximum power point tracking control of wind turbine based on two-mass model without anemometer. Frontiers in Energy Research 2021;9:584.

[24] Badihi H, Zhang YM, Hong H. Fuzzy gain-scheduled active fault-tolerant control of a wind turbine. Journal of the Franklin Institute 2014;351(7):3677-3706.

[25] Shao H, Gao ZW, Liu XX, Busawon K. Parameter-varying modelling and fault reconstruction for wind turbine systems. Renewable Energy 2018;116:145-152.

[26] Xiahou KS, Li MS, Liu Y, Wu QH. Sensor fault tolerance enhancement of DFIG-WTs via perturbation observer-based DPC and two-stage Kalman filters. IEEE Transactions on Energy Conversion 2018;33(2):483-495.

[27] Kamal E, Aitouche A, Ghorbani R, Bayart M. Robust fuzzy fault tolerant control of wind energy conversion systems subject to sensor faults.

IEEE Transactions on Sustainable Energy 2012;3(2):231-241.

[28] Liu XX, Gao ZW, Chen ZQ. Takagi-Sugeno fuzzy model based fault estimation and signal compensation with application to wind turbines. IEEE Transactions on Industrial Electronics 2017;64(7):5678-5689.

[29] Jlassi I, Cardoso AJM. Fault-tolerant back-to-back converter for direct-drive PMSG wind turbines using direct torque and power control techniques. IEEE Transactions on Power Electronics 2019;34(11):11215-11227.

[30] Rahimilarki R, Gao ZW, Zhang AH, Binns R. Robust neural network fault estimation approach for nonlinear dynamic systems with applications to wind turbine systems. IEEE Transactions on Industrial Informatics 2019;15(12):6302-6312.

[31] Li MS, Yu D, Chen ZM, Xiahou KS, Ji TY, Wu QH. A data-driven residual-based method for fault diagnosis and isolation in wind turbines. IEEE Transactions on Sustainable Energy 2019;10(2):895-904.

[32] Zhao HS, Liu HH, Hu WJ, Yan XH. Anomaly detection and fault analysis of wind turbine components based on deep learning network. Renewable Energy 2018;127: 825-834.

[33] Azizi A, Nourisola H, Shoja-Majidabad S. Fault tolerant control of wind turbines with an adaptive output feedback sliding mode controller. Renewable Energy 2019;135:55-65.

[34] Li DY, Cai WC, Song YD, Chen HJ. Adaptive fault tolerant control of wind turbines with guaranteed transient performance considering active power control of wind farms. IEEE Transactions on Industrial Electronics 2018;65(4):3275-3285.

[35] Boukhezzar B, Siguerdidjane H. Nonlinear control of a variable-speed wind turbine using a two-mass model. IEEE Transactions on Energy Conversion 2011;26(1):149-162.

[36] Ren YX, Li LY, Brindley J, Jiang L. Nonlinear PI control for variable pitch wind turbine. Control Engineering Practice 2016;50:84-94.

[37] Zouheyr D, Lotfi B, Abdelmadjid B. Improved hardware implementation of a TSR based MPPT algorithm for a low cost connected wind turbine emulator under unbalanced wind speeds. Energy 2021;232:121039.

[38] Jiang L, Wu QH, Wen JY. Decentralized nonlinear adaptive control for multimachine power systems via high-gain perturbation observer. IEEE Transactions on Circuits and Systems I: Regular Papers 2004;51(10):2052-2059.

[39] Jiang L, Wu QH. Nonlinear adaptive control via sliding-mode state and perturbation observer. IEE Proceedings-Control Theory and Applications 2002;149(4):269-277.

[40] Han JQ. From PID to active disturbance rejection control. IEEE Transactions on Industrial Electronics 2009;56(3):900-906.

[41] Chen J, Jiang L, Yao W, Wu QH. Perturbation estimation based nonlinear adaptive control of a full-rated converter wind turbine for fault ride-through capability enhancement. IEEE Transactions on Power Systems, 2014, 29(6): 2733-2743.

[42] Chen J, Yao W, Ren YX, Wang RT, Zhang LH, Jiang L. Nonlinear adaptive speed control of a permanent magnet synchronous motor: A perturbation estimation approach. Control Engineering Practice 2019;85:163-175.